ISIJ International, Vol. 59 (2019), No. 11, pp. 2098–2104

Effects of Fine Precipitates on Austenite Grain Refinement of Micro-alloyed Steel during Cyclic Heat Treatment

Genki SAITO,[1)]* Norihito SAKAGUCHI,[1)] Munekazu OHNO,[1)] Kiyotaka MATSUURA,[1)] Masayoshi TAKEUCHI,[2)] Taichi SANO,[2)] Koki MINOGUCHI[2)] and Takuya YAMAOKA[2)]

1) Faculty of Engineering, Hokkaido University, Sapporo, 060-8628 Japan.
2) Mitsubishi Steel MFG. Co., Ltd., Tokyo, 290-0067 Japan.

(*Received on March 18, 2019; accepted on May 17, 2019; J-STAGE Advance published date: July 30, 2019*)

The effects of fine precipitates on the austenite grain refinement of micro-alloyed steel during cyclic heat treatment were investigated under different solution treatments. After three rounds of cyclic heat treatment of A_{c3} and A_{r3} transformations of the as-received steel rod with rapid heating and cooling, the austenite grain size was 3–10 μm. On the other hand, three rounds of cyclic heat treatment after solution treatment at 1 300°C reduced the austenite grain size to 2–5 μm. The as-received sample included AlN–Ti(C,N)–MnS composite particles with a mean diameter of 30 nm and a number density of 11 μm^{-3}, and the mean diameter did not change during cyclic heat treatment. Thus, it was considered that the reduction in austenite grain size without solution treatment was caused by the increase in the nucleation site of austenite phase with increasing number of cycles, due to the refinement of the prior austenite grains with martensitic structure during the cyclic heat treatment. When solution-treated at 1 300°C, the AlN–Ti(C,N)–MnS composite particles were solved, and they were precipitated during the cyclic heat treatment with a mean diameter of 12 nm and an increased number density of 85 μm^{-3}. Thus, it was considered that the further reduction in austenite grain size with solution treatment was caused by the pinning effect of the fine precipitates, in addition to the increase in the number of austenite phase nucleation sites with increasing number of heat treatment cycles.

KEY WORDS: grain refinement; reverse transformation; cyclic heat treatment; precipitation.

1. Introduction

Weight reduction is a key factor in automobile fuel efficiency improvement and consequently CO_2 emission reduction. This weight reduction is applicable to all automobile parts, including suspension components such as coil springs and leaf springs. For weight reduction of spring steels, it is essential to improve their mechanical strength and toughness. One effective means of improving the mechanical strength and toughness of steels is the grain refinement of austenite (γ), according to the Hall-Petch relationship.[1)] This relationship is generally applicable not only to yield stress, but also to ultimate tensile stress and cleavage fracture toughness.[2)] The grain refinement of steels can be achieved via various methods, such as cyclic heat treatment,[3–6)] micro alloying,[7–12)] ausforming,[13)] recrystallization after large strain deformation,[14)] mechanical milling,[14)] accumulative roll-bonding,[15)] and so on. From the viewpoints of applicability to mass production and economic efficiency, micro alloying and cyclic heat treatment are the most promising methods.

It has been shown that the addition of small amounts of Al, V, Nb, Ti, and N, called "micro alloying," results in the dispersion of fine precipitates of carbide, nitride, and carbo-nitride, such as AlN, V(C,N), Nb(C,N) and Ti(C,N) in steel.[7–12)] These precipitates then act as pinning particles, preventing grain growth. Selecting a suitable heat treatment is key to achieving uniformly distributed fine precipitates. In general, as-solidified steel contains coarse precipitates, which are fully or partially solved during a hot-rolling or heating process. Subsequently, precipitation occurs during cooling after the solution treatment, re-heating, or aging process, where the heating conditions greatly affect the precipitation behavior. It is known that continuous gradual cooling after hot-rolling often generates coarse inhomogeneous precipitates. In contrast, when a sample is re-heated at lower temperature after quenching from high temperature, fine homogeneous precipitates tend to be formed because of the increased nucleation frequency under a high degree of supersaturation.[10,16,17)]

Cyclic heat treatment has been applied to the spheroidizing of cementite[18)] and the grain refinement of steels.[3–6)] Grange first reported that cyclic heat treatment of steel through the Ac_1 to Ac_3 range could reduce its γ grain size, where the sample was rapidly heated and cooled within 3 min.[5)] For effective grain refinement, the maximum heat treatment temperature should be kept relatively low (but

* Corresponding author: E-mail: genki@eng.hokudai.ac.jp
DOI: https://doi.org/10.2355/isijinternational.ISIJINT-2019-153

higher than the temperature of complete austenization), and quenching should be performed immediately after heat treatment. In the case of AISI 8640 steel (Ni–Cr–Mo-alloyed carbon steel), the γ grain size was reduced to 3.3 μm after four rounds of rapid cyclic heat treatment.[5,19] Because the grain boundary of the former phase acts as the nucleation site of the new phase, the finer initial γ grain size reduces the final γ grain size.[20] Thus, cyclic heat treatment can reduce the γ grain size. In addition, rapid cooling from austenite to martensite is considered to accelerate the nucleation rate and reduce the γ grain size.[6]

As mentioned above, micro alloying and cyclic heat treatment are considered to be effective methods of steel grain refinement. However, the effects of fine precipitates on grain refinement in the case of combined micro alloying and cyclic heat treatment remain unclear, in spite of the industrial importance of this method. Therefore, the relationships between γ grain size and fine precipitates were investigated in this study under different solution treatments and different cyclic heat treatments of micro-alloyed spring steels. In addition, the mean diameter, number density, and volume fraction of fine precipitates were quantitatively analyzed via transmission electron microscopy (TEM), including direct observation and thickness evaluation.

2. Experimental Procedures

The spring steel used in this study was a micro-alloyed JIS SUP-12 steel, 0.55C-1.55Si-0.8Mn-0.001S-0.8Cr-0.025Al-0.003Ti-0.003N (in mass%). The sample was hot-rolled and then annealed at 900°C for 1 h. The steel was a 15-mm-diameter rod, which was sectioned in the forging direction to obtain rod-like samples with dimensions of ϕ3 mm × L10 mm. Each rod-like sample was cyclically heat-treated as shown in **Fig. 1**, using a heating transformation measurement apparatus (Formastor-F, Fuji Electronic Industrial Co., Ltd.). The heating of each sample, from room temperature to 780°C, was repeated three times; some samples were solution-treated at either 1 100°C or 1 300°C for 20 s before the cyclic heat treatment. The heating and cooling were performed within 20 s. The cyclic heat-treated samples were sectioned in the transverse direction, mechanically polished, and etched by 4 mass% picric acid solution at 323 K. The microstructure of each section was observed via scanning electron microscopy (SEM, ProX, Phenom-World B.V.).

The precipitates in each sample were investigated using a scanning transmission electron microscope (STEM, Titan^3 G2 60–300, FEI Company). To prepare the STEM samples, disc-like samples cut from the rod-like samples were polished down to a thickness of $<$20 μm and ion-milled with 5 kV Ar ions using a precision ion polishing system (PIPS, model 691, Gatan Inc.). High-angle annular dark field (HAADF) imaging was employed for observation. To avoid the effects of diffraction, a large acceptance angle of the STEM detector between 126 and 200 mrad was used. The probe current was set to around 0.35 nA. To analyze the number density and volume fraction of the precipitates, the sample thickness at each observed area was quantitatively estimated via electron energy loss spectroscopy (EELS). For the thickness calibration, three samples, with different thicknesses ranging from 80 to 300 nm, were prepared using a focused ion beam-equipped SEM (FIB-SEM, JIB-4600F/HKD, JEOL), and low-loss spectra obtained via EELS were calibrated using the known thicknesses of these samples. The thermodynamic phase calculation was performed using Thermo-Calc software version 2018b, with the TCFE9 database.[21]

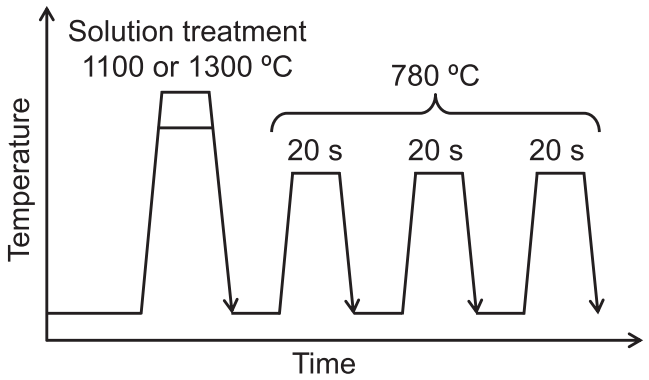

Fig. 1. Heat pattern of the cyclic heat treatment.

3. Results and Discussion

Figure 2 shows SEM images of γ grain structures obtained at different heat treatments. As the number of the cycles increases, the grain size decreases in samples both with and without solution treatment. The as-received rod was slowly cooled after annealing; thus, the microstructure of the as-received sample consisted of pearlite colonies, ranging in size from 30 to 40 μm. **Table 1** summarizes the γ grain size under each condition. After one round of cyclic heat treatment without solution treatment, γ grains with sizes of 3–30 μm formed. The three rounds of cyclic heat treatment reduced the grain size to 3–10 μm. Although not shown here, further cyclic heat treatment did not result in substantial changes in grain size. When the as-received sample was solution-treated at 1 100°C and subjected to three rounds of cyclic heat treatment, the γ grain size decreased slightly, to 2–10 μm. After solution treatment at 1 300°C, the γ grain size ranged from 200 to 300 μm, as shown in Fig. 2(d). The sample after one round of cyclic heat treatment had a duplex microstructure consisting of fine and coarse grains with a grain size ranging from 2 to 60 μm, and three rounds of heat treatment brought about a homogeneous, small grain size range of 2–5 μm. Thus, it was found that a combination of a high-temperature solution treatment and repeated cyclic heat treatment was highly effective for γ grain refinement. The low-temperature heat treatment after the high-temperature solution treatment resulted in the precipitation of fine second-phase particles, which strongly retarded the grain boundary migration, as pinning particles are known to do.

To investigate the effects of the heat treatment on the precipitation state of the pinning particles, the precipitates were investigated via SEM and TEM. **Figures 3**(a) and 3(b) show SEM images of the as-received sample, which were acquired using backscattered electron composition imaging. The observed texture corresponds to the channeling contrast of subgrains. Coarse MnS and Ti(C,N) precipitates with sizes of 100–300 nm are evident in the as-received

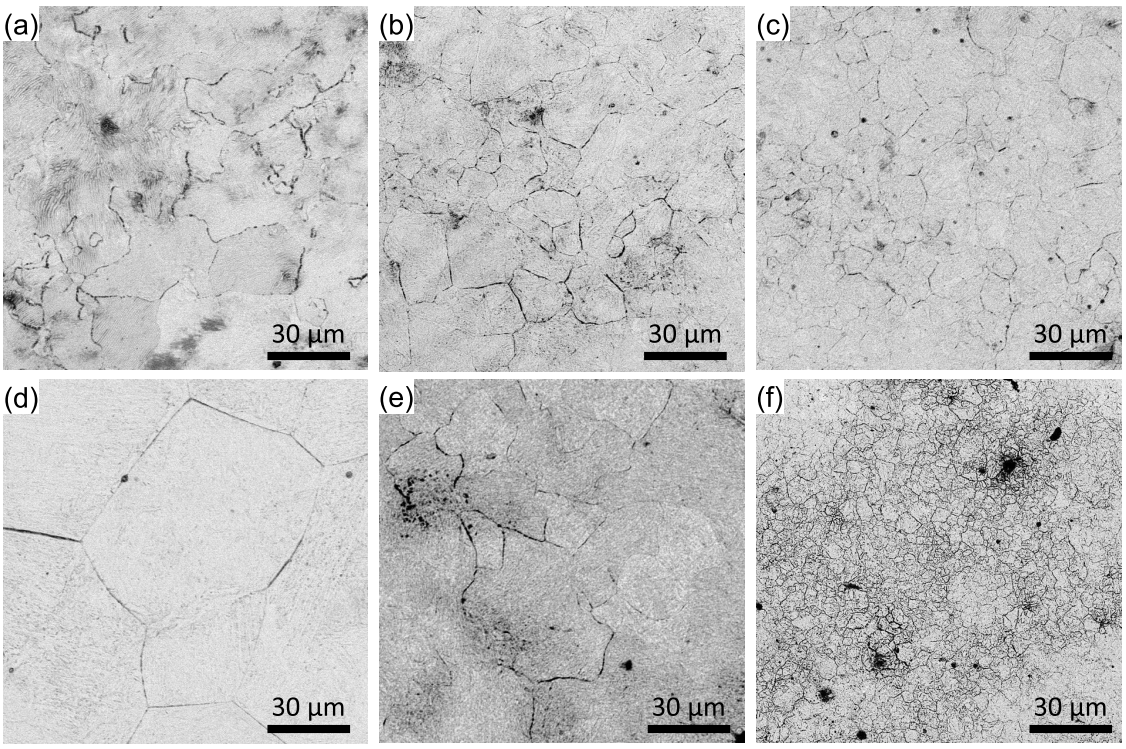

Fig. 2. SEM images of samples (a) as-received, (b) 780°C × 1, (c) 780°C × 3, (d) solution-treated at 1 300°C, (e) 780°C × 1 after 1 300°C solution treatment, and (f) 780°C × 3 after 1 300°C solution treatment.

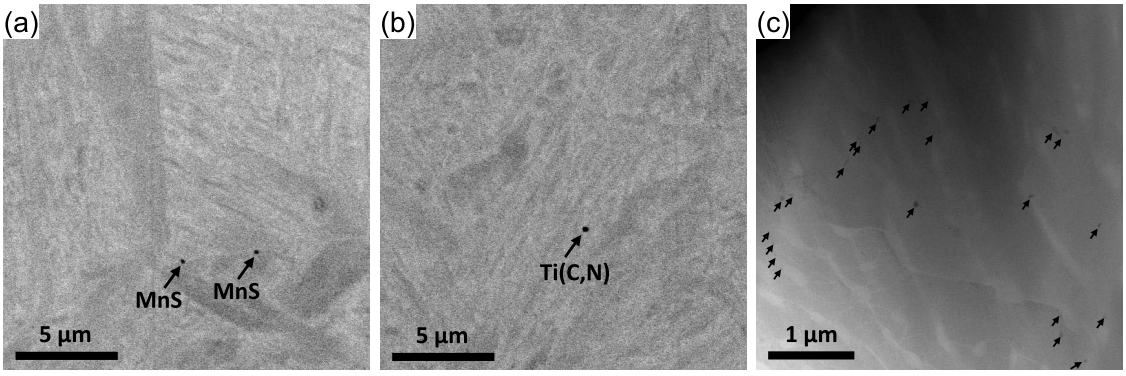

Fig. 3. (a, b) SEM images and (c) HAADF-STEM image of the as-received sample.

Table 1. γ grain size range under each heating condition.

780°C × 1	3–30 μm
780°C × 3	3–10 μm
1 100°C + 780°C × 3	2–10 μm
1 300°C	200–300 μm
1 300°C + 780°C × 1	2–60 μm
1 300°C + 780°C × 2	3–30 μm
1 300°C + 780°C × 3	2–5 μm

sample. It is considered that these coarse precipitates were formed during a hot rolling or annealing process. Figure 3(c) shows an HAADF-STEM image of the as-received sample. The striped bright contrast in Fig. 3(c) corresponds to the cementite phase in a perlite structure, where Mn, Cr, and C were concentrated. Precipitates with sizes of around 30 nm are visible, as indicated by the arrows in Fig. 3(c), and these small precipitates are significantly more numerous than the coarse particles observed by SEM. **Figures 4**(a) and 4(e) show the enlargement of these small precipitates in the as-received samples and the corresponding energy dispersive spectroscopy (EDS) mappings for Figs. 4(b)–4(d) and Figs. 4(f)–4(h), respectively. It is clearly evident that the precipitates consisted of Al, Ti, and Mn. Based on further investigation via elemental mapping of S and N as well as electron diffraction, these particles were found to be AlN, Ti(C,N), and MnS. In most cases, these particles had combined with each other to form AlN–Ti(C,N)–MnS composite particles. It is considered that these particles precipitated during cooling after the hot rolling or annealing step. Because several kinds of precipitates can be generated at lower temperature, composite particles often form in steels.[16] It has previously been reported that the precipitation of AlN can be enhanced by the existence of MnS because the interfacial energy between AlN and MnS is small.[22]

The number density, mean diameter, and volume frac-

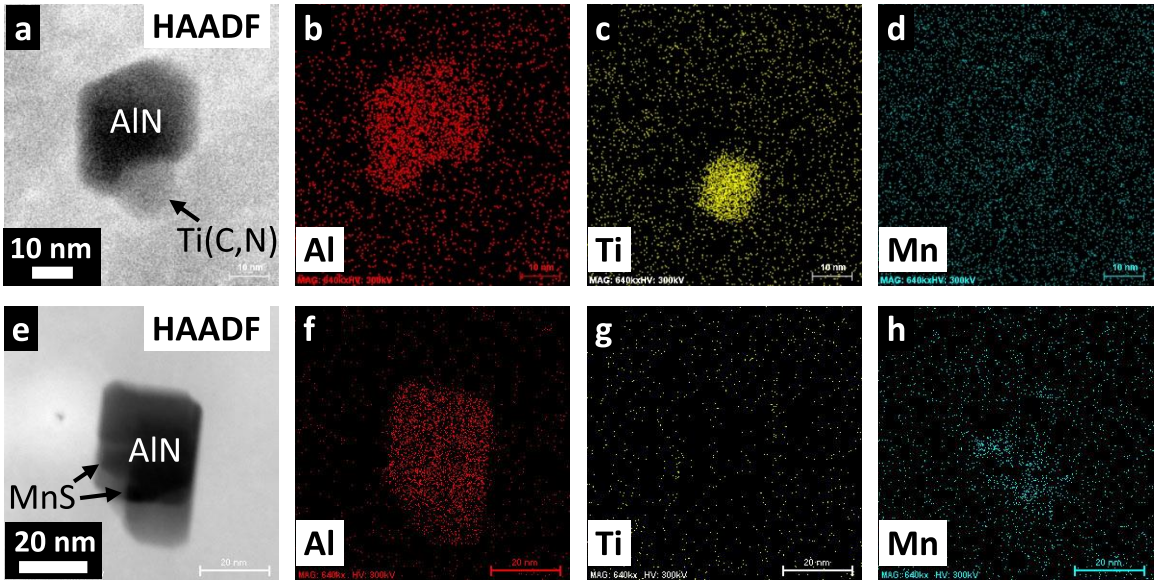

Fig. 4. HAADF-STEM images and corresponding STEM-EDS mapping of the as-received sample. (Online version in color.)

Table 2. Number density, mean diameter, and volume fraction of precipitates obtained from STEM analysis.

Sample	Number density, μm^{-3}	Mean diameter, nm	Volume fraction
As received	11	33	0.040%
780°C × 1	11	27	0.027%
780°C × 3	7	33	0.023%
1 100°C	7	21	0.008%
1 300°C	–	–	–
1 300°C + 780°C × 1	4	< 10	0.005%
1 300°C + 780°C × 3	85	12	0.014%

tion of the precipitates, obtained from STEM analysis, are summarized in **Table 2**. The coarse precipitates observed by SEM were not included for these analyses because their number density was quite low. The number density and volume fraction were obtained by calculating the absolute sample thickness at each observed area, using the calibrated low-loss EELS data. Here, the mean diameters indicate the whole diameters of the composite particles including different kinds of precipitates. The number density and mean diameter of the as-received sample were 11 μm^{-3} and 33 nm, respectively, and these values were not significantly affected by three rounds of cyclic heat treatment. Therefore, it is considered that almost equilibrium amounts of the precipitates had already formed in the as-received sample. When the cyclic heat treatment was repeated three times, the γ grain size slightly decreased from 3–30 to 3–10 μm, as shown in Table 1. Since the size and amount of precipitates did not significantly change after three rounds of cyclic heat treatment without solution treatment, the slight decrease in γ grain size after the cyclic treatment should be ascribed not to a change in the pinning effect, but rather to the increased nucleation of γ grains during the cyclic heat treatment. It has been reported that because the grain boundary of the former phase acts as a nucleation site for the new phase, the

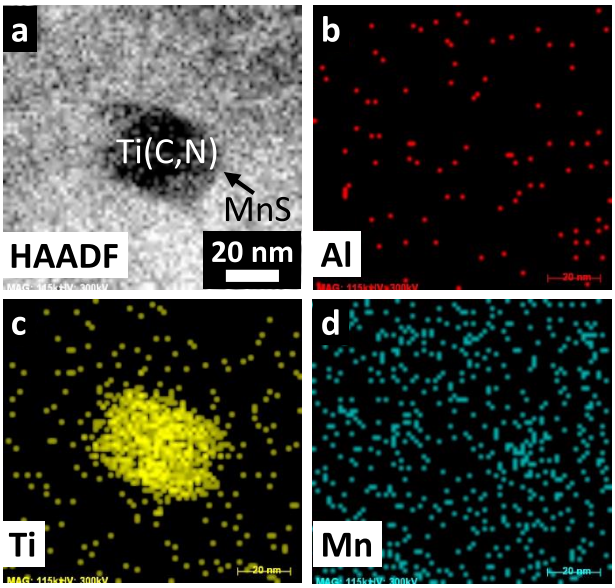

Fig. 5. (a) HAADF-STEM image and (b–d) corresponding STEM-EDS mapping of the sample solution-treated at 1 100°C. (Online version in color.)

refinement of the initial γ grain size results in refinement of the final γ grain size.[20]

Figure 5 shows a HAADF-STEM image and corresponding STEM-EDS mappings of the sample solution-treated at 1 100°C. A cubic-shaped Ti(C,N) particle can be seen, whereas AlN is not observable. According to the thermodynamic calculation results shown in **Fig. 6** and **Table 3**, AlN disappeared at 1 100°C, while Ti(C,N) and MnS existed at this temperature. As shown in Table 2, the mean size and number density of the precipitates slightly decreased in the sample solution-treated at 1 100°C compared to those in the as-received sample, which should be due to the decrease in AlN.

Figure 7 shows HAADF-STEM images of the sample after solution treatment at 1 300°C, followed by cyclic heat treatment. After solution treatment at 1 300°C, no

precipitates were observed in the sample before cyclic heat treatment (Fig. 7(a)), and fine particles with sizes of around 10 nm were observed in the cyclic heat-treated sample. The number of precipitates increased with increasing number of cycles (Figs. 7(b) and 7(c)). When the number of cycles increased from one to three, the number density of the precipitates increased from 4 to 85 μm^{-3}, which is greater than that of the precipitates without solution treatment (7–11 μm^{-3}), as shown in Table 2. The EDS analysis results shown in **Fig. 8** reveal that these precipitates are composite particles, including AlN, Ti(C,N), and MnS particles. Compared to the precipitates of the as-received sample shown in Fig. 4, the MnS particles are clearly visible. In the case of the as-received sample, the coarse MnS particles initially grew at high temperature and AlN was precipitated at lower temperature during gradual cooling after the hot rolling process and subsequent annealing process. In contrast, the precipitation of AlN, Ti(C,N), and MnS occurred simultaneously in the solution-treated sample, which is considered to be a reason for the increased MnS in the fine precipitate. In particular, the precipitates after one round of cyclic heat treatment after solution treatment at 1 300°C mainly consisted of MnS particles. According to the thermodynamic calculation results shown in Fig. 6, MnS is much more supersaturated than AlN, implying that MnS precipitates first, followed by AlN and finally Ti(C,N)–MnS–AlN combined particles. In the case of the as-received sample, precipitation occurred during cooling after the hot rolling or annealing step, and the mean size of the precipitates was around 30 nm. The mean size of the solution-treated sample, on the other hand, was reduced to 10 nm, which might be related to the fine MnS generation at 780°C.

It should be noted that the number density of the precipitates increased from 4 to 85 μm^{-3} when the number of the cycles increased from one to three and that precipitates of AlN and Ti(C,N)–AlN composite without MnS attachment were observed in the sample after solution treatment at 1 300°C and three rounds of cyclic heat treatment. If the initially nucleated MnS acted as a nucleation site for further precipitation of AlN and Ti(C,N), the number density of the precipitates might not increase dramatically, and all precipitates should contain the MnS core. However, as already described, precipitates without MnS attachment were observed in the sample after three rounds of cyclic heat treatment, which suggests that a new nucleation site for further precipitation might be generated during every heat treatment cycle. If the precipitation mainly occurred after reverse transformation to γ during cyclic heat treatment, the γ grain boundaries could be possible candidates for the precipitate nucleation sites, and the cyclic heat treatment with α-γ transformation could generate numerous new γ grain boundaries during each heating cycle. In addition, dislocations might also act as nucleation sites for the precipitates. It was previously reported that grain boundaries and dislocations in austenite can act as nucleation sites for MnS precipitation in 3% Si steel and that deformation at high temperature can accelerate MnS precipitation.[23] When the quenched sample was heated, precipitation could also occur in the martensite during heating. In this case, the

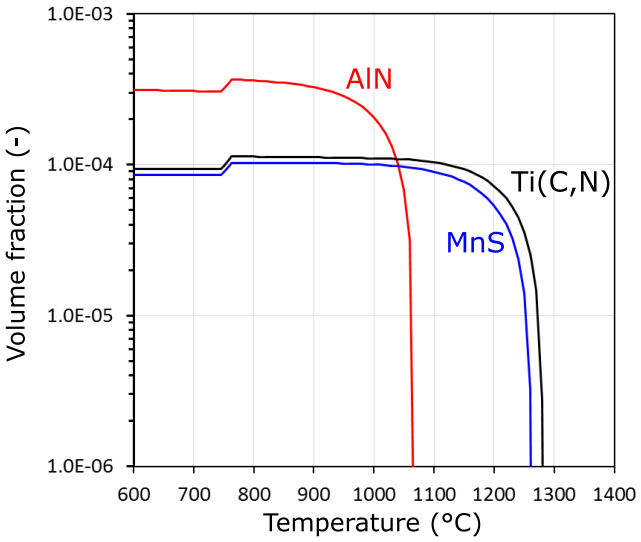

Fig. 6. Volume fraction of each precipitate determined by performing thermodynamic calculations. (Online version in color.)

Table 3. Summary of volume fractions at 780°C and solution temperature of each precipitate as determined by performing thermodynamic calculations.

	AlN	Ti(C,N)	MnS	Total
Volume fraction at 780°C	0.0365%	0.0113%	0.0103%	0.0581%
Solution temperature	1 068°C	1 282°C	1 263°C	

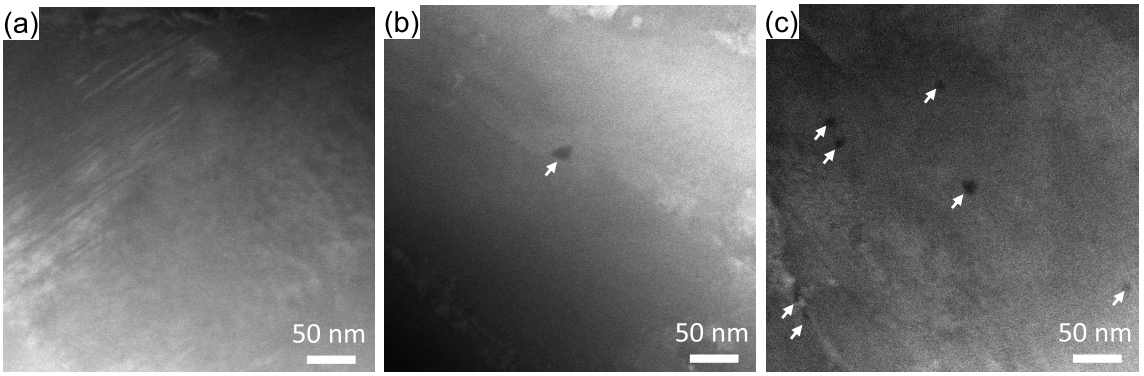

Fig. 7. HAADF-STEM observations of (a) solution-treated at 1 300°C, (b) 780°C × 1 after solution treatment, and (c) 780°C × 3 after solution treatment.

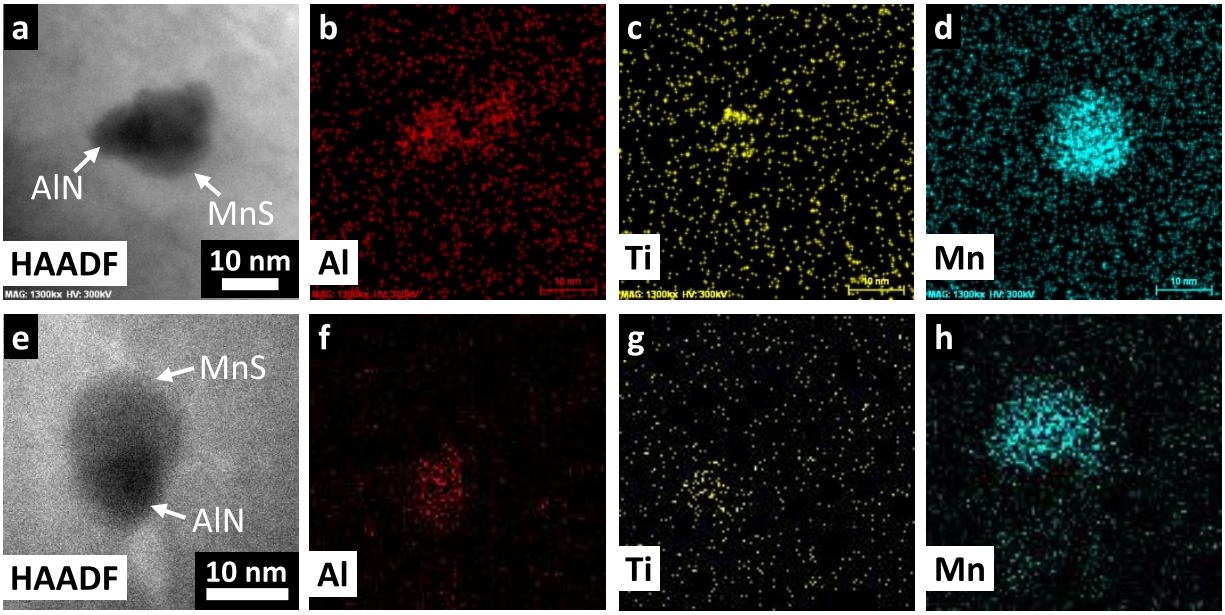

Fig. 8. HAADF-STEM images and corresponding STEM-EDS mapping for (a–d) 780°C × 1 after 1 300°C solution treatment and (e–h) 780°C × 3 after 1 300°C solution treatment. (Online version in color.)

Table 4. γ grain sizes estimated using the Zener equation (Eq. (1)).

	Diameter of precipitate	Volume fraction	Measured γ grain size	Estimated γ grain size
(a)	33 nm	0.023%	3–10 μm	24.4 μm
(b)	12 nm	0.014%	2–5 μm	14.6 μm
(c)	12 nm	0.058%	–	3.5 μm

sub-grain boundary is a possible nucleation site for precipitation. The increase in the amount of fine precipitates after solution treatment at 1 300°C and three rounds of cyclic heat treatment is considered to have been achieved by the increased number of precipitate nucleation sites generated by cyclic heat treatment, although the precipitate nucleation site remains unclear.

In summary, based on the results displayed in Tables 1 and 2, it appears that cyclic heat treatment is effective for γ grain refinement and that solution treatment increases the effects of the cyclic heat treatment because of the precipitation of fine particles, which suppress the grain growth of the γ phase nucleated by cyclic heat treatment.

Finally, let us discuss the effect of pinning on the γ grain structure. Table 3 summarizes the volume fraction at 780°C and solution temperature of each precipitate, according to thermodynamic calculations. The total volume fraction for AlN, Ti(C,N), and MnS at 780°C is 0.0581%, which is larger than the measured values for the samples after three treatment cycles, both with and without solution treatment, as shown in Table 2. The volume fraction of precipitates in the sample after three heat treatment cycles after solution treatment at 1 300°C is 0.014%, which is low compared to the volume fraction of 0.023–0.040% observed in the samples without solution treatment. Hence, the complete precipitation of nitride and sulfide particles cannot be achieved only by the present cyclic treatment. It is expected that a strong effect of pinning on γ grain growth may be obtained by promoting the precipitation of pinning particles. This point is discussed below based on the Zener pinning model.

When the grain growth is completely inhibited by the particle pinning, the grain size can be calculated by using the Zener equation, Eq. (1),[24] and the results obtained in this manner were then compared to the measured results.

$$d = K\frac{r}{f_V} \quad \text{..... (1)}$$

The Zener equation is generally used to describe the effects of the average radius of the pinning particles, r, and the volume fraction of the particles, f_V, on the average grain diameter, d, using a constant, K. $K = 0.34$ was used in this study, because the pining effect of γ grains by nitrides or carbides can be reproduced well with this value.[11,25] **Table 4** shows the γ grain sizes calculated using Eq. (1), and the measured values are also shown for comparison. Table 4 (a) and (b) correspond to the sample without solution treatment and the sample with solution treatment at 1 300°C respectively. The estimated γ grain sizes are 24.4 and 14.6 μm for the samples without and with solution treatment, respectively. These calculated values are larger than the measured value ranges of 3–10 and 2–5 μm, respectively. The decrease in γ grain size should be ascribed to the increased γ grain nucleation during the cyclic heat treatment. In addition, complete pinning did not occur in the present experiments and further γ grain structure refinement could be achieved by enhancing the pinning effect. For instance, when the precipitation of the pinning particles is completed, the average grain size is expected to decrease from 14.6 to 3.5 μm according to the calculations performed using the Zener equation (see (b) and (c) in Table 4).

4. Conclusions

In this study, the relationships between austenite grain size and fine precipitates were investigated under different solution treatments and cyclic heat treatments of A_{c3} and

A_{r3} transformations, for micro-alloyed spring steels. The following conclusions were obtained:

(1) The austenite grains in the as-received steel rod were refined to 3–10 μm in diameter after three rounds of cyclic heat treatment at 780°C, while 1 300°C solution treatment followed by three rounds of cyclic heat treatment reduced the austenite grain size to 2–5 μm.

(2) The as-received sample included AlN–Ti(C,N)–MnS composite precipitate particles, with a mean diameter of 33 nm and a number density of 11 μm^{-3}. After 1 300°C solution treatment and three rounds of cyclic heat treatment at 780°C, the mean diameter of the precipitates decreased to 12 nm and their number density increased to 85 μm^{-3}.

(3) Cyclic heat treatment after solution treatment was effective for austenite grain refinement owing to the precipitation of fine particles, which suppressed the growth of austenite grains nucleated during the cyclic heat treatment.

Acknowledgements

The authors would like to thank M. Eng. Ms. Yukiko Tanaka and Dr. Eng. Ms. Toko Tokunaga for their extensive experimental support. We gratefully acknowledge Mr. Kenji Ohkubo, Mr. Ryo Ota, Dr. Sc. Mr. Takashi Endo, Mr. Takashi Tanioka, M. Eng. Ms. Ryoko Kurishiba, Ms. Emiko Obari, and M. MedSc. Ms. Ami Matsuno for their technical assistance with the TEM operations and sample preparations. A part of this work was conducted at Hokkaido University, supported by the "Nanotechnology Platform" Program of the Ministry of Education, Culture, Sports, Science, and Technology (MEXT), Japan.

REFERENCES

1) E. O. Hall: *Proc. Phys. Soc. Sect. B*, **64** (1951), 747.
2) D. A. Curry and J. F. Knott: *Met. Sci.*, **10** (1976), 1.
3) A. Kościelna and W. Szkliniarz: *Mater. Charact.*, **60** (2009), 1158.
4) R. A. Grange: *Metall. Trans.*, **2** (1971), 65.
5) R. Grange: *ASM Trans. Q.*, **59** (1966), 26.
6) H. Nozaki, Y. Nishikawa, Y. Uesugi and I. Tamura: *Tetsu-to-Hagané*, **72** (1986), 1598 (in Japanese).
7) C. M. Enloe, K. O. Findley and J. G. Speer: *Metall. Mater. Trans. A*, **46** (2015), 5308.
8) K. A. AlOgab, D. K. Matlock, J. G. Speer and H. J. Kleebe: *ISIJ Int.*, **47** (2007), 1034.
9) Y. Kurebayashi and S. Nakamura: *Denki Seiko* (*Electr. Furn. Steel*), **65** (1994), 67.
10) T. Murakami, H. Hatano and H. Yaguchi: *Tetsu-to-Hagané*, **92** (2006), 448 (in Japanese).
11) M. Sasaki, K. Matsuura, K. Ohsasa and M. Ohno: *Tetsu-to-Hagané*, **94** (2008), 491.
12) M. Chapa, S. F. Medina, V. López and B. Fernández: *ISIJ Int.*, **42** (2002), 1288.
13) X. Sun, Z. Li, Q. Yong, Z. Yang, H. Dong and Y. Weng: *Sci. China Technol. Sci.*, **55** (2012), 1797.
14) K. Tomimura, S. Takaki and Y. Tokunaga: *ISIJ Int.*, **31** (1991), 1431.
15) N. Tsuji, Y. Saito, H. Utsunomiya and S. Tanigawa: *Scr. Mater.*, **40** (1999), 795.
16) T. Takamiya and O. Furukimi: *Tetsu-to-Hagané*, **100** (2014), 1413 (in Japanese).
17) T. Obara, H. Takeuchi, T. Takamiya and T. Kan: *J. Mater. Eng. Perform.*, **2** (1993), 205.
18) Z.-q. Lü, H.-f. Zhang, Q. Meng, Z.-h. Wang and W.-t. Fu: *J. Iron Steel Res. Int.*, **23** (2016), 145.
19) T. Tsumura, Y. Kamada, S. Tanoue and H. Ohtani: *Tetsu-to-Hagané*, **70** (1984), 1993 (in Japanese).
20) Y. Mukaida, T. Shibata, S. Ono and T. Ishiguro: *Tetsu-to-Hagané*, **86** (2000), 472 (in Japanese).
21) Thermo-Calc Software: Thermo-Calc Software TCFE9 Database, https://www.thermocalc.com/, (accessed 2018-10-01).
22) K. Ushioda, H. G. Suzuki, H. Komatsu and K. Esaka: *J. Jpn. Inst. Met.*, **59** (1995), 373.
23) T. Takamiya, T. Obara, M. Muraki and M. Komatsubara: *Tetsu-to-Hagané*, **89** (2003), 518 (in Japanese).
24) N. A. Haroun and D. W. Budworth: *J. Mater. Sci.*, **3** (1968), 326.
25) P. A. Manohar, M. Ferry and T. Chandra: *ISIJ Int.*, **38** (1998), 913.